Low-Temperature Deposition of Silicon Oxide Film from the Reaction of Silicone Oil Vapor and Ozone Gas

Susumu HORITA*, Koichi TORIYABE, and Kensuke NISHIOKA†

School of Materials Science, Japan Advanced Institute of Science and Technology, 1-1 Asahidai, Tatsunokuchi, Ishikawa 923-1292, Japan

Using the chemical reaction between silicone oil vapor and ozone gas at atmospheric pressure and above 200 ^{o}C, we deposited a Si oxide film. Fourier transformer infrared (FT-IR) spectra of the films were very similar to those of thermal SiO_2 films without peaks due to carbon for deposition temperatures T_s from 200 to 350 ^{o}C. Although a small peak due to the Si-OH bond appeared for $T_s \leq 300$ ^{o}C, it was reduced with increasing T_s and almost disappeared around 350 ^{o}C. Secondary ion mass spectrometry measurements showed that the concentrations of metal and carbon impurities were at a negligible level for device performance even for $T_s = 200$ ^{o}C. The dielectric property of the film deposited at 350 ^{o}C was also shown to be comparable to the SiO_x film produced by a conventional low-temperature deposition method, although the estimated density of interface trap was in the order of $10^{11}/(cm^2 \cdot eV)$.

* E-mail address: horita@jaist.ac.jp

† Present address: Department of Applied Physics, University of Miyazaki, 1-1 Gakuen Kibanadai Nishi, Miyazaki 889-2192, Japan.

1. Introduction

Low-temperature deposition of silicon oxide films is desired for high-quality gate oxide films to obtain high-performance low-temperature (< 500 ^{o}C) polycrystalline silicon (LTPS) thin film transistors (TFTs) on nonheat-resistant glass.[1)] The TFT performance strongly depends on the SiO_2/Si interface properties. A low-temperature process is also needed to form interlayer dielectrics (ILD) in size-minimizing integrated circuit to suppress the disconnection of interconnect metal, redistribution of dopant, and defect generation in the fabricated underlayer.[2)] Currently, for this requirement, by using tetraethylorthosilicate [TEOS: $Si(OC_2H_5)_4$] gas or TEOS/ozone (O_3), plasma enhanced chemical vapor deposition (PECVD) process and thermal CVD process have come into practical use.[3-6)]

On the other hand, siloxane polymers or silicones have also been used as starting materials to produce silicon oxide films at low temperatures. They are promising materials because of their low cost and high safety compared with TEOS.[7)] The price per unit volume of silicone oil (SO) is much lower than that of TEOS by about one order. TEOS is toxic to human eyes and throats while silicone is a safe material. In fact, silicone rubbers are often embedded in human bodies after surgical operations. Reports have appeared that a Si oxide film was deposited from gaseous molecules generated from a solid target of silicone rubber using ArF (193 nm) or F_2 (157 nm) laser irradiation.[8,9)] Amorphous Si oxide networks have been formed by photoinduced reactions of polysiloxane films using UV excimer laser irradiation at room temperature.[10)] Furthermore, there are many reports of the transformation of poly dimethylsiloxane (PDMS) into thin films of SiO_x by exposure to UV/O_3 at room temperature, where O_3 was produced by exposure of atmospheric oxygen to UV irradiation.[12,13)] In the UV/O_3 method, thin layers of PDMS were prepared by Langmuir-Blodgett or spin-coating techniques. However, these SiO_x layers are too thin for applications in TFTs and ILDs in LSI, and they contain nonnegligible carbon content,

probably more than 1%.

In contrast, for deposition of Si oxide film, we used SO ($[SiO(CH_3)_2]_nO[Si(CH_3)_3]_2$) vapor as a source in CVD and allowed it to react with O_3 gas at temperatures above 200 ^oC.[14,15] Thus far, there has been no report that SO vapor may be used as a source instead of solid or liquid silicone material. In this paper, we show that we can obtain silicon oxide film even at 200 ^oC by this method, and show the Fourier transformer infrared (FT-IR) spectra of the films. Depth profiles of impurity concentrations are also shown for carbon (C), sodium (Na), and others, which strongly affect the electrical properties of Si devices. The impurities were measured by secondary ion mass spectrometry (SIMS). Furthermore, the dielectric properties of deposited films were measured and compared with those of a film produced by CVD with TEOS as a source, and the interface properties with the Si substrate were also estimated. We discuss these experimental results, in particular, the FT-IR data, in detail. Hereafter, Si oxide films formed by SO vapor and O_3 gas are called SO oxide films.

2. Experimental Procedure

Figure 1 shows a schematic diagram of the atmospheric pressure (AP) CVD system used for the deposition of SO oxide films in this study. The substrates were n-type single crystals with a resistivity of 1-10 Ω·cm. The crystallographic orientation of the substrate was (111) because it has been reported that the low-temperature crystallized Si films, e.g., those produced by excimer laser annealing, are preferentially (111)-oriented.[16,17] They were chemically cleaned in hot acid solution and dipped in dilute HF solution to remove the Si oxide. The chemically cleaned substrates were loaded in the quartz tube reactor, which was uniformly heated at an average temperature or deposition temperature T_s from 200 to 350 ^oC. The diameter of the quartz tube

was 36 mm, and the heater zone was between the distances *X* of 300 and 600 mm from the gas inlet. The SO (GE Toshiba Silicones TSF451-10, kinematic viscosity 10 mm^2/s) was vaporized directly by bubbling with N_2 gas at a flow rate of 0.8 slm through a Teflon tube heated to about 60 ^oC to avoid condensation of SO vapor. The ozone (1-5%) was generated by a silent electric discharge from 99.9995% O_2 gas at a flow rate of 0.7 slm and then introduced into the reactor together with the SO vapor. These gas flow rates of N_2 and O_2 were primarily used in this study; when other flow rates are used, they will be mentioned specifically. The film thicknesses and refractive indexes of the as-deposited films were measured by ellipsometry, and molecular structures were analyzed from FT-IR spectra collected at a resolution of 1 cm^{-1}. Impurity concentrations of hydrogen (H) and C, and of metals of iron (Fe), nickel (Ni), Na, and potassium (K), were measured by SIMS for the films deposited at T_s=200 and 350 ^oC, respectively. The metal-oxide-semiconductor (MOS) structures (Al/SO oxide/(111)Si) were fabricated by depositing Al films as top electrodes on the samples, where the diameter was 100 μm. Then, the current density-electric field (J-E) characteristics and the capacitance-voltage (C-V) characteristics at 1 MHz were measured. Before the electrical measurements, postmetallization annealing (PMA) in N_2 atmosphere for 30 min was performed to improve the interface properties.

3. Results

Ozone is well-known to be thermally decomposed into O_2+O,[18,19] which is an important elementary process for the formation of SO oxide films in our system. We investigated the relationship between the degree of ozone decomposition and deposition temperature T_s. We monitored the residual ozone gas exhausted from the outlet using an ozone monitor without

silicone oil vapor, where the concentration of O_3 gas introduced was ~1%. Figure 2 shows the dependence of the ozone residual ratio on T_s. The residual ratio was calculated by dividing the O_3 concentration monitored in the outlet by the concentration introduced. From this figure, it can be seen that the ozone residual ratio begins to decrease at T_s = 150 ^oC, and that most of the ozone gas is thermally decomposed above 200 ^oC in our system. A similar behavior was observed under the other gas flow conditions of N_2 /O_2 = 0.35/1.15 slm and N_2/O_2 = 1.15/0.35 slm.

Figure 3 shows the actual temperature profiles in the reactor and the distributions of the deposition rate R_d of the SO oxide films, where the horizontal axis is the distance from the gas inlet, X, as shown in Fig. 1, and the parameters are deposition temperatures T_s. It can be seen from this figure that the actual temperatures increase around X = 300 mm and decrease around 600 mm abruptly; these positions correspond to the edges of the heater. Also, the uniform temperature zone is between 350 and 550 mm from the inlet, where the fluctuation in temperature was $\pm$5 ^oC around T_s. For any T_s, R_d increases rapidly near 170 ^oC, at which temperature the ozone begins to decompose actively, as shown in Fig. 2. The distribution forms of R_d are Gaussian-like with a tail as reported for the TEOS/O_3 system.[3-5] Since the shape of the distribution is closely related to the actual temperature profile, the relationship between distribution and temperature is discussed later.

Figure 4 shows the FT-IR spectra of SO and the SO oxide films deposited at T_s=200, 250, 300, and 350 ^oC, compared with the 50-nm-thick thermal Si oxide (SiO_2) film formed by dry oxygen at 1050 ^oC. We selected the SO oxide films deposited near the highest R_d positions in Fig. 3 for each T_s. The thicknesses for 200, 250, 300, and 350 ^oC were approximately 220, 390, 340, and 350 nm, respectively. As can be seen in the SO spectrum, the peaks due to C-H and Si-CH_3 bonds appear at around 3000 and 1060 cm^{-1}, respectively. However, in the spectra of the SO

oxide films, these peaks disappear. The patterns are also similar to that of the thermal SiO_2 film. The peaks at around 1070 and 840 cm^{-1} of the SO and thermal SiO_2 films are identified as absorptions due to a bending (TO_2) mode and an asymmetric stretching (TO_3) mode, respectively, of the Si-O-Si bond.[20-23] We can say from this result that the SO oxide films are almost stoichiometric silicon oxide. However, in the films deposited at 200, 250, and 300 ^oC, peaks due to Si-OH bonds are observed around 960 cm^{-1}, and the intensities decrease with increasing T_s. This means that the SO oxide films contain relatively large amounts of water, and the contents are reduced by increasing T_s, which is similar to many reports of Si oxide films formed by other low-temperature deposition methods.[3-5,24,25] On the other hand, from the SO oxide film at 350 ^oC, the peak due to Si-OH bonds is much reduced and hardly observed, which means that the film contains little water. By carefully comparing the peaks due to the TO_3 mode in the SO oxide films with the various T_s, it is found that the peak wavenumbers are lower than that of the standard thermal oxide film and that the downward shift is enhanced by increasing T_s. The widths of the peaks increase with T_s. It is known that the TO_3 mode peak is more sensitive to film structure, including the Si-O-Si bond angle θ, the composition ratio between Si and O, film density, and so on, compared with peaks due to the other modes.[21-23, 26] The film structure is discussed in more detail later.

Another significant difference from the thermal SiO_2 film is the high intensity of the shoulder around 1200 cm^{-1} in the SO oxide films. Since it has been claimed that the intensity of the shoulder increases as density decreases or porosity increases,[27,28] the result indicates that the SO oxide films are more porous and structurally less ordered.

Figures 5(a) and 5(b) show the FT-IR spectra of the SO oxide films deposited at T_s = 200 and 350 ^oC, respectively, where the parameter is deposition position X. From both figures, it can

be seen that the peak position is almost independent of X. The dependence of FWHM on X is also not as great as on T_s in Fig. 4. Actually, the variations in FWHM for T_s = 200 and 350 ^oC in Fig. 5 were smaller than 4 and 9 cm^{-1}, respectively. This means that the film structure is mainly governed by T_s and is not so influenced by thermal and chemical reactions during the transport of the reaction gases from the inlet to the outlet. On the other hand, in Fig. 5(a) for T_s = 200 ^oC, the peaks due to Si-OH bond are clearly observed irrespective of the deposition position X. However, in Fig. 5(b) for T_s = 350 ^oC, although a weak and broad peak due to Si-OH bond appears at X = 36 mm, it gradually decreases with X and is hardly observed beyond X = 42 mm. The behavior of this peak is discussed further as well as the TO_3 mode peak in a later section.

Here, we consider the deposition mechanism of the SO oxide film from the viewpoint of a thermal reaction between SO vapor and O_3 gas, which is similar to that of the TEOS/O_3 system.[3-5,29,30] As shown in Fig. 2, ozone gas is decomposed thermally into O_2+O. The chemically very active O atoms react with -CH_3 side groups of SO in the gas phase and intermediate products (precursors) are formed together with the by-products H_2O and CO_2. In other words, -CH_3 side groups are substituted with hydroxyl –OH, and silanol bonds of Si-OH cover the sides of the siloxane chains. The surface of the Si substrate or the deposited Si oxide film is terminated by -OH due to exposure to O_3 gas. The -OH groups on the surface are eliminated by a dehydration reaction with -OH groups on the precursors, Si-OH(surface) + -OH(precursor) $\rightarrow$Si-O-Si +H_2O. Then, a $[\text{-Si-O-Si-}]_n$ network is constructed on the substrate and the deposition of Si oxide film continues. When the deposition temperature for dehydration reaction is so low that all -OH bonds can not be removed from the precursor during the deposition, the FT-IR peaks due to Si-OH bonds are observed from the SO oxide films deposited at $T_s \leq 300$ ^oC, as shown in Fig. 4. In contrast, at 350 ^oC, the dehydration reaction is so active

that the deposited films contain few –OH groups.

Figure 6(a) shows the SIMS depth profiles of metals Fe, Ni, Na, and K in the SO oxide film deposited at T_s = 350 ^{o}C. As one can see from this figure, the impurities of Fe and Ni are at the background level (BL) in the film. On the other hand, the concentrations of alkali metals Na and K decrease exponentially with depth, and they reach BL in the Si substrate. Alkali metals are abundant in the environment. In fact, the human body is one of the major sources of Na contamination. It is suggested that the signals of Na and K result from ions adsorbed on the sample during transport from the deposition system to the SIMS measurement system. It is also well-known that the analysis of mobile elements such as Na, K, and Li by SIMS is influenced by the migration of the elements due to the electric field during the measurements, and it is not easy to obtain accurate depth distributions.[31,32)] The broad peak of Na in the vicinity of the interface between the SO oxide film and Si substrate is caused by the so-called matrix effect.[33)]

Figure 6(b) shows the SIMS depth profiles of C and H in the SO oxide film deposited at T_s = 200 ^{o}C compared with the secondary ion intensities of Si and O as references. From this figure, it can be seen that the concentration of C is relatively low, about 10^{19} cm^{-3}, regardless of the low deposition temperature of 200 ^{o}C, and that it is comparable to the reported value of a TEOS oxide film.[34)] This means that most of carbons in SO are eliminated by reaction with O_3 even at 200 ^{o}C. On the contrary, the H concentration is high as predicted from the FT-IR spectra in Figs. 4 and 5. The signals from H originate from water and OH in the deposited SO oxide film. The broad peak of C around the interface is due to a matrix effect like that for Na. From the results shown in Figs. 6(a) and 6(b), we can say that the impurities in the oxide film made from SO are negligible for device performance, except for H.

Figure 7 shows current density-electric field characteristics of the SO oxide film (solid line) deposited at T_s = 350 ^{o}C after postdeposition annealing (PDA) at 350 ^{o}C for 1 h in N_2, where the

PMA temperature was 350 ^{o}C. We selected the sample deposited at X = 44 mm and further away from the highest R_d position because it had fewer OH groups. The characteristics are compared with those of the TEOS oxide film (dotted line) produced by electron cyclotron resonance (ECR) PECVD. [5)] From this figure, it can be seen that, although the leakage current of the SO oxide film is larger than that of thermal SiO_2 in general, it is comparable with that of the ECR-PECVD film. However, the dielectric properties of the SO oxide films deposited at $T_s \leq 300$ ^{o}C, even after 300 ^{o}C PDA for 6 h and 300 ^{o}C PMA, were so poor that the leakage currents were more than 10^{-6} A/cm^2 even at 2 MV/cm. This poor quality is probably caused by water or OH impurities contained in the film, as shown in the FT-IR spectra of Figs. 4 and 5(a) and in the SIMS profile of Fig. 6(b).

It is also noted from the SO oxide film in Fig. 7 that spikelike currents appear below 5 MV/cm. As one of the causes, we can suggest a well-known "self-healing effect",[36-38)] in which material is removed from the Al electrode by the breakdown and then the device returns to the low-conductivity state. Breakdowns occur at defects like pinholes in silicon oxide films. It has been reported that surfaces of the Si oxide films deposited by CVD with TEOS/O_3 gases become rough if the surface during deposition is terminated with few silanol OH groups,[5,29)] because the OH groups contribute to the growth of the Si oxide films through dehydration as mentioned previously. More OH groups result in high growth rate and smooth film surfaces, but fewer lead to the evolution of rough surfaces. Rougher films sometimes contain a number of voids and defects like pinholes. Since, for the SO oxide film in Fig. 7, the deposition temperature and deposition rate are high, 350 ^{o}C, and low, ~1 nm/min, respectively, the number of OH groups terminating the growth surface during deposition may not be sufficient to produce a smooth surface. If the self-healing effect is the main cause of the spikelike current, the breakdown field is strictly below 1 MV/cm. However, the intrinsic dielectric strength of SO oxide film can be as

high as that of the conventional PECVD oxide films without pinholelike defects.

Figure 8 shows the C-V characteristics of the SO oxide film deposited at T_s = 350 ^oC (open circles) of the same sample as in Fig. 7, compared with the thermal SiO_2 film grown at 1050 ^oC (closed circles) and the theoretical curve (solid line) of the ideal MOS structure. The film thickness was about 14 nm. As one can see from this figure, the hysteresis loops are hardly observed in both samples. However, the curve of the SO oxide film apparently slants more than that of the thermal SiO_2 film and the theoretical curve. This result suggests that the SO oxide film contains few mobile charged ions, but it has a relatively large density of interface trap (DIT) compared with the thermal SiO_2 film. The DIT estimated by the Terman method was about $(3\text{-}5)\times10^{11}/(cm^2\cdot eV)$, which is not a good level for use as gate oxide. This relatively high DIT indicates an imperfect and defective interface, and the possible reasons are as follows; the deposition temperature is not as high for chemical reaction between Si and O as for the thermal oxidation, and a small number of -OH groups near the interface affects the construction near the interface to produce the poor electrical properties. The flat-band voltage V_f for the thermal SiO_2 film and the SO oxide film are about -0.53 and -0.37 V, respectively, which are different from the ideal value of -0.201 V with a flat-band capacitance of 6.0 pF. The major reason for the deviation from the ideal value is considered to be the (111) crystallographic orientation of the Si substrate used. It is well-known that the orientation of the minimum fixed charge density is (100) for Si, but the maximum is (111), whose dependence is similar to that of DIT.[39,40] If it is assumed that shift in V_f from the ideal, ΔV_f, is caused by the effective fixed charge per unit area Q_f, Q_f/q is calculated to be $\sim4.7\times10^{11}$ cm^{-2} from ΔV_f = -0.53 V- (-0.201 V) ≈ -0.33 V for the thermal SiO_2 film, where q is an elementary charge. This value is comparable to the reported one of $\sim5.6\times10^{11}$ cm^{-2} for the (111) surface.[40] It should be noted that the ΔV_f of the SO oxide film

being smaller than that of the thermal SiO_2 is not due to smaller Q_f but to higher DIT. The higher DIT makes the C-V curve stretch out more along the horizontal axis of applied voltage, which also causes a positive shift in V_f for an n-type Si substrate.

4. Discussion

At first, using the deposition model for SO oxide film, we can explain the position dependence of the deposition rate R_d of the deposited film, which is shown in Fig. 3. The deposition region is almost consistent with the region of O_3 decomposition. Thermal decomposition of O_3 is promoted by increasing T_s, as shown in Fig. 2. At higher T_s, most of the decomposition occurs within the narrower region of the reactor, where the region is shifted more toward the inlet with increasing T_s. Therefore, as T_s increases, the peak position of R_d moves toward the inlet. The other intermediate products or precursors that do not contribute to the major deposition diffuse and flow with the carrier gas toward the outlet. Then, in the downstream region, they fall down and are transformed into Si oxide to contribute to the deposited film, which results in the tail of the distribution.

Next, we discuss the wavenumber and full width at half maximum (FWHM) of the peak due to the TO_3 mode. In Fig. 4, the definitions of wavenumber and FWHM are given.[22,23,27] The FWHM contains two components: one arises from the broadening of the low-frequency and dominant component of the line (TO_3 mode), and the other is from the shoulder at high wavenumbers. The wavenumber k_i of the ideal peak due to the TO_3 mode can be calculated from $k_i = k_0 \sin\theta$, where $k_0 = 1116.5$ cm^{-1} for $\theta = 150^o$.[23] Assuming k_0 is constant for any deposition condition in our study, a positive or negative shift of k from the standard peak indicates positive or negative change in θ from the standard bonding angle.[22,23] The width of the peak can also be

understood in terms of a statistical distribution of θ and summation over narrow angles. Therefore, if FWHM is small, the distribution of θ is narrow, and vice versa. In the case of physically densified or thermal SiO_2 film, when the oxidation temperature is lower, the peak is shifted to a lower wavenumber. The density of the thermal SiO_2 film formed at lower temperature increases, which can be verified by the increase in the refractive index. The film densification induces stress in the film, and the bonding angle θ is decreased. Therefore, a downward shift of wavenumber for thermal SiO_2 film indicates densification of the film.[22,23] However, in the case of films deposited at low temperatures, this relationship is not always applicable[41] because such films are generally porous. In fact, the refractive indices of the SO oxide films in this study were lower, 1.42 to 1.46, than that of the thermal oxide film, 1.46. This is supported by the results in Figs. 4 and 5 that show higher intensity of the shoulder around 1200 cm^{-1}. It has also been reported that the wavenumbers and FWHM of peaks of thermal SiO_2 films increase with thickness, and that the increment becomes saturated as the films become thicker than 40 nm.[23] In the case of Fig. 4, since the thickness of the thermal SiO_2 film is over 50 nm, we can use the wavenumber and FWHM of its peak as references for comparison to the SO oxide films. Since the thicknesses of the SO films in Fig. 4 are more than 200 nm, the dependences of wavenumber and FWHM of the peak on thickness can be generally ignored.

Figure 9 shows the dependences of the wavenumber and FWHM of the peak due to the TO_3 mode on T_s from the data in Fig. 4. It can be seen from this figure that the wavenumber and FWHM of the peak decrease and increase, respectively, with increasing T_s. Many reports indicate that the wavenumbers of the peaks of the Si oxide films produced by a low-temperature process are lower than that of thermal SiO_2 film.[41-44] The relationship between the wavenumber of peak and θ suggests to us that θ of all the samples is smaller than that of thermal SiO_2 and that

increasing T_s causes θ to decrease. Some researchers commented that the downward shift for low-temperature Si oxide film indicates higher film strain in spite of the porosity of the film, compared with that of the high-temperature thermal SiO_2 film.[27,28,43] Chou and Lee reported the FT-IR spectra of the Si oxide films prepared using liquid-phase deposition (LPD) at 50 ^oC.[28] They observed complicated behavior of the TO_3 mode peak when the annealing temperature was increased to 200, 400, 600, and 800 ^oC. By increasing it from 200 to 600 ^oC, the peak shifted to lower wavenumber and broadened. However, by further increasing the temperature to 800 ^oC, the direction of the peak shift was opposite, i.e., to higher wavenumber and the peak became sharp, because the film strain is relaxed or relieved by high annealing temperature over 800 ^oC. The tendency below 600 ^oC is similar to our case. Reports have also shown that the FWHM depends on the low-temperature deposition process and the values vary, e.g., smaller or larger than that of thermal SiO_2.[27,28, 42-44] Taking these reports into account, the results in Fig. 9 can be explained as follows; at the low T_s of 200 ^oC, the thermal vibration of the atoms composing the SO oxide film is insufficient to relax the strain in the low-temperature-formed Si-O network, so the film is stressed and the variation in θ is limited. By raising T_s, the bond strength between Si and O atoms is enhanced, which makes the film strain stronger as a whole. However, the vibration of atoms is still insufficient to relax the stress, even at higher T_s. As a result, the average angle is reduced, but the distribution spreads, so that the peaks shift to low wavenumbers and the FWHM increase in the FT-IR spectra.

Further, we consider the dependence of the intensity of the FT-IR peak on deposition position due to Si-OH bonds shown in Fig. 5(b). Because the decomposition of O_3 gas and dehydration reaction are much more active at T_s = 350 ^oC than at T_s = 200 ^oC, we can obtain the local and highest R_d at 350 ^oC as shown in Fig. 3. Around the inlet side of the highest R_d position

at T_s = 350 ^oC, the higher deposition rate does not allow sufficient process time to remove OH groups completely from the absorbed precursors through dehydration reactions. Further, the dehydration reaction at the inlet side may be less active than at the outlet side near the highest R_d position because the local temperature in the reactor actually increases with distance from the inlet to near X = 50 mm, as shown in Fig. 2. Therefore, at X = 36 mm, the deposited SO film contains a measurable number of OH groups. In spite of the high R_d region at the outlet side, higher local temperature and longer transport time of the precursors may enhance dehydration to reduce the number of OH groups in the film.

5. Conclusions

We deposited Si oxide films on Si substrates using the reaction between SO vapor and O_3 gas at 200 to 350 ^oC. The FT-IR spectra showed that the films deposited from 200 to 350 ^oC are almost stoichiometric Si oxides without signals related to C, although small signals due to water and OH bonds appeared in the films deposited at $T_s \leq 300$ ^oC. The spectra also suggested that the films were strained in spite of their slight porosity compared with the thermal SiO_2 film. Taking the FT-IR results into account, we considered the deposition mechanism to be similar to the TEOS/O_3 system, and discussed the results in more detail using this model. The SIMS depth profiles showed that the impurity concentrations of metals and C are at a negligible level for device performance. The dielectric properties of the 350 ^oC SO oxide film are also comparable to those of a film produced from a TEOS source, although the interface properties between SO oxide and Si are inadequate. From these results, it can be said that SO vapor can be used currently as a deposition source in CVD for low-temperature deposition of SO oxide film except for the application of gate oxide. However, the interface properties may be much improved by future investigations about the formation mechanism of the interface, optimization of fabrication

and PDA conditions, and other issues. From an industrial point of view, we still have a few serious issues. The deposition rate is too low, e.g., 1 nm/min at T_s = 200 ^{o}C and 3 nm/min at 350 ^{o}C. Water and OH groups, which cause poor dielectric properties, are contained in the SO oxide films deposited at low temperatures ≤ 300 ^{o}C. In order to find solutions for these issues, a new deposition method with SO as a source may be needed.

Acknowledgment

The authors gratefully acknowledge Professor Y. Kawakami at the Japan Advanced Institute of Science and Technology for useful comments.

References

1) S. Higashi, D. Abe, S. Inoue, and T. Shimoda: Jpn. J. Appl. Phys. **40** (2001) 4171.

2) M. M. Moslehi, R. A. Chapman, M. Wong, A. Paranjpe, H. N. Najm, J. Kuehne, R. L. Yeakley, and C. J. Davis: IEEE Trans. Electron Devices **39** (1992) 4.

3) M. Matsuura, Y. Hayashide, H. Kotani, and H. Abe: Jpn. J. Appl. Phys. **30** (1991) 1530.

4) T. Kawahara, A. Yuuki, and Y. Matsui: Jpn. J. Appl. Phys. **31** (1992) 2925.

5) M. Yoshimaru and T. Yoshie: J. Electrochem. Soc. **145** (1998) 2847.

6) J. Arnó, Z. Yuan, and S. Murphy: J. Electrochem. Soc. **146** (1999) 276.

7) H. Nakashima, K. Omae, T. Takebayashi, C. Ishizuka, and T. Uemura: J. Occup. Health **40** (1998) 270.

8) M. Okoshi, M. Kuramatsu, and N. Inoue: Jpn. J. Appl. Phys. **40** (2001) L41.

9) H. Takao, M. Okoshi, and N. Inoue: Jpn. J. Appl. Phys. **42** (2003) L461.

10) O. Joubert, G. Hollinger, C. Fiori, R. A. B. Devine, P. Paniez, and R. Pantel: J. Appl. Phys. **69** (1991) 6647.

11) C. L. Mirley and J. T. Koberstein: Langmuir **11** (1995) 1049.

12) M. Ouyang, C. Yuan, R. J. Muisener, A. Boulares, and J. T. Koberstein: Chem. Mater. **12** (2000) 1591.

13) F. D. Egitto and L. J. Matienzo: J. Mater. Sci. **41** (2006) 6362.

14) T. Toriyabe, K. Nishioka, and S. Horita: Proc. 13th Int. Display Workshops (IDW'06), 2006, p. 719.

15) S. Horita, K. Toriyabe, and K. Nishioka: Proc. 14th Int. Display Workshops (IDW'07), 2007, p. 1865.

16) S. Christiansen, P. Lengsfeld, J. Krinke, M. Nerding, N. H. Nickel, and H. P. Strunk: J. Appl.

Phys. **89** (2001) 5348.

17) K. Brendel, P. Lengsfeld, I. Sieber, A. Schöpke, N. H. Nickel, W. Fuhs, M. Nerding, and H. P. Strunk: J. Appl. Phys. **91** (2002) 2969.

18) J. V. Michael: J. Chem. Phys. **54** (1971) 4455.

19) M. O. Popovich, G. V. Egorova, and Y. V. Filippov: Russ. J. Phys. Chem. **59** (1985) 165.

20) F. L. Galeener: Phys. Rev. B **19** (1979) 4292.

21) P. G. Pai, S. S. Chao, Y. Takagi, and G. Lucovsky: J. Vac. Sci. Technol. A **4** (1986) 689.

22) G. Lucovsky, M. J. Manitini, J. K. Srivastava, and E. A. Irene: J. Vac. Sci. Technol. B **5** (1987) 530.

23) J. T. Fitch, G. Lucovsky, E. Kobeda, and E. A. Irene: J. Vac. Sci. Technol. B **7** (1989) 153.

24) N. Hirashita, S. Tokitoh, and H. Uchida: Jpn. J. Appl. Phys. **32** (1993) 1787.

25) K. Murase, N. Yabumoto, and Y. Komine: J. Electrochem. Soc. **140** (1993) 1722.

26) M. Nakamura, Y. Mochizuki, K. Usami, Y. Itoh, and T. Nozaki: Solid State Commun. **50** (1984) 1079.

27) R. M. Almeida and C. G. Pantano: J. Appl. Phys. **68** (1990) 4225.

28) J.-S. Chou and S.-C. Lee: J. Appl. Phys. **77** (1995) 1805.

29) D. Cheng, K. Tsukamoto, and H. Komiyama: J. Appl. Phys. **85** (1999) 7140.

30) S. Romet, M. F. Couturier, and T. K. Whidden: J. Electrochem. Soc. **148** (2001) G82.

31) R. A. Kushner, D. V. McCaughan, V. T. Murphy, and J. A. Heilig: Phys. Rev. B **10** (1974) 2632.

32) R. Saito and M. Fudo: Jpn. J. Appl. Phys. **37** (1998) 690.

33) R. G. Wilson, F. A. Stevie, and C. W. Magee: *Secondary Ion Mass Spectrometry* (Wiley, New York, 1989) Chap. 2.3.

34) N. Kodama, H. Mori, S. Saito, and K. Koyama: Nucl. Instrum Methods Phys. Res. B **118**

(1996) 505.

35) D. Abe, S. Higashi, S. Inoue, T. Shimoda, T. Morimura, and K. Saito: Jpn. J. Appl. Phys. **42** (2003) L814.

36) N. Klein: IEEE Trans. Electron Devices **13** (1966) 788.

37) C. M. Osburn and D. W. Ormond: J. Electrochem. Soc. **119** (1972) 591.

38) M. Av-Ron and M. Shatzkes: Appl. Phys. Lett. **21** (1972) 233.

39) E. Arnold, J. Ladell, and G. Abowitz: Appl. Phys. Lett. **13** (1968) 413.

40) E. H. Nicollian and J. R. Brews: *MOS (Metal Oxide Semiconductor) Physics and Technology* (Wiley, New York, 1982) Chap. 15.4.

41) C. Martinet and R. A. B. Devine: J. Appl. Phys. **77** (1995) 4343.

42) P. Lange: J. Appl. Phys. **66** (1989) 201.

43) P. Lange, U. Schnakenberg, S. Ullerich, and H.-J. Schliwinski: J. Appl. Phys. **68** (1990) 3532.

44) A. Barranco, F. Yubero, J. Cotrino, J. P. Espinós, J. Benítez, T. C. Rojas, J. Allain, T. Girardeau, J. P. Rivière, and A. R. González-Elipe: Thin Solid Films **396** (2001) 9.

Figure captions

Fig. 1 (Color online)

Schematic drawing of the APCVD system used for the deposition of Si oxide films using SO vapor and $O_2 + O_3$ gas. The SO vapor was produced by bubbling SO with N_2 gas.

Fig. 2

Dependence of ozone residual ratio in the exhausted gas on average temperature or deposition temperature T_s. The ozone gas concentration ratio of the introduced gas, O_3/O_2, was ~1%.

Fig. 3

Temperature profiles and deposition rate R_d distributions of the SO films in the reactor for the deposition temperatures of T_s = 200, 250, 300, and 350 ^oC.

Fig. 4 (Color online)

FT-IR spectra of SO and the SO oxide films deposited at T_s = 200, 250, 300, and 350 ^oC, compared with the thermal oxide SiO_2 film.

Fig. 5 (Color online)

FT-IR spectra of the SO oxide films deposited at T_s = 200 ^oC (a) and 350 ^oC (b) as a function of the deposition position X. The vertical dotted lines are visual guides.

Fig. 6 (Color online)

(a) SIMS depth profiles of metals Fe, Ni, Na, and K in the SO oxide film deposited at T_s = 350 ^oC on the Si substrate. (b) SIMS depth profiles of C and H, in reference to Si and O secondary ion intensities in the SO oxide film deposited at T_s = 200 ^oC on the Si substrate.

.

Fig. 7 (Color online)

Current density-electric field characteristics of the SO oxide film deposited at T_s = 350 ^oC from the SO source, followed by PDA of 300 ^oC in N_2 for 1 h and PMA of 350 ^oC in N_2 for 30 min, compared with the Si oxide film deposited at 400 ^oC by ECR-PECVD from TEOS source as a reference.

Fig. 8 (Color online)

C-V characteristics of the SO oxide film deposited at T_s = 350 ^oC for the same sample as in Fig. 7, compared with the thermal oxide film grown at 1050 ^oC. The film thickness was about 14 nm.

Fig. 9

Deposition temperature T_s dependences of the peak wavenumber and FWHM of the peaks due to asymmetry stretching (TO_3) mode of Si-O-Si bond. The values of thermal Si oxide film are indicated by the broken lines.

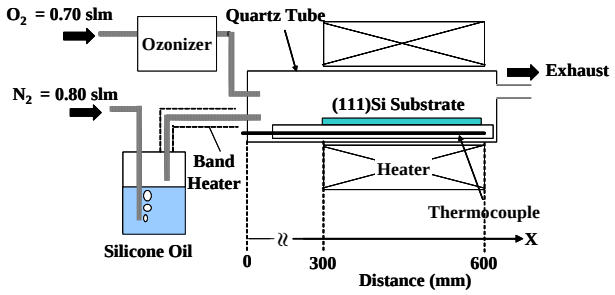
O2 = 0.70 slm
Ozonizer
Quartz Tube
Exhaust
N2 = 0.80 slm
(111)Si Substrate
Band
Heater
Heater
Thermocouple
Silicone Oil
0
300
600
X
Distance (mm)

Fig. 1

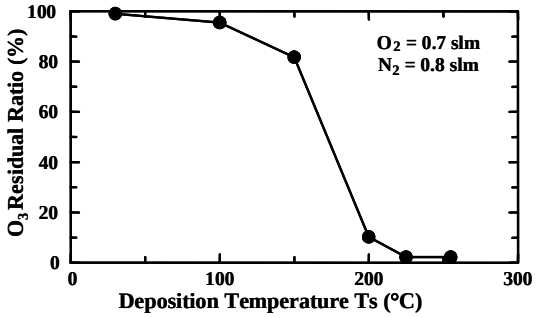
100
80
60
40
20
0
0
100
200
300
O3 Residual Ratio (%)
Deposition Temperature Ts (°C)
O2 = 0.7 slm
N2 = 0.8 slm

Fig. 2

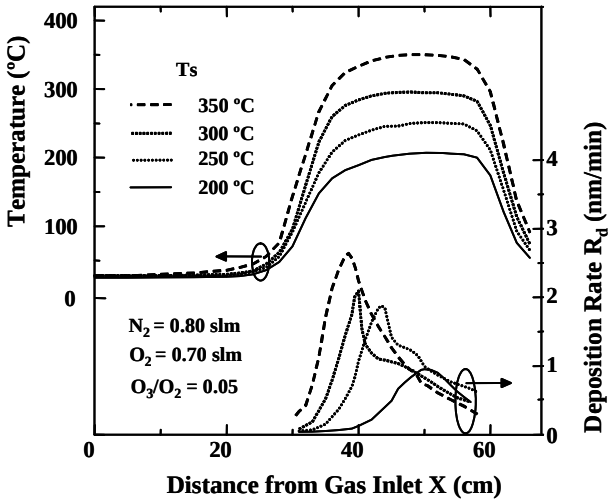
Temperature (°C)
Deposition Rate R_d (nm/min)
Distance from Gas Inlet X (cm)
Ts
350 °C
300 °C
250 °C
200 °C
N_2 = 0.80 slm
O_2 = 0.70 slm
O_3/O_2 = 0.05
400
300
200
100
0
4
3
2
1
0
0
20
40
60

Fig. 3

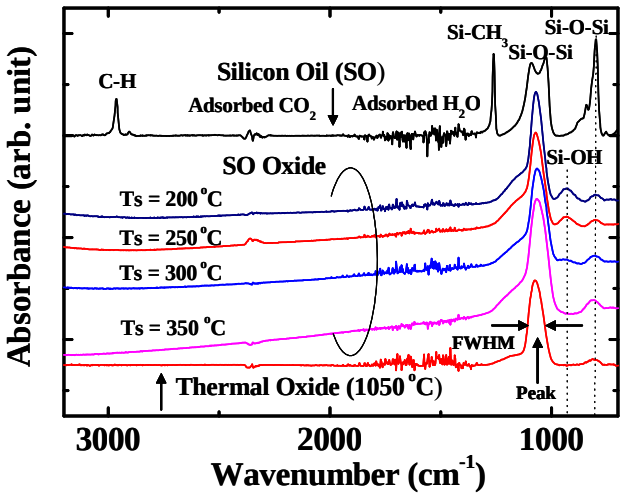
Absorbance (arb. unit)
Wavenumber (cm-1)
3000
2000
1000
C-H
Silicon Oil (SO)
Adsorbed CO2
Adsorbed H2O
Si-CH3
Si-O-Si
Si-O-Si
Si-OH
SO Oxide
Ts = 200°C
Ts = 250°C
Ts = 300°C
Ts = 350°C
Thermal Oxide (1050°C)
FWHM
Peak

Fig. 4

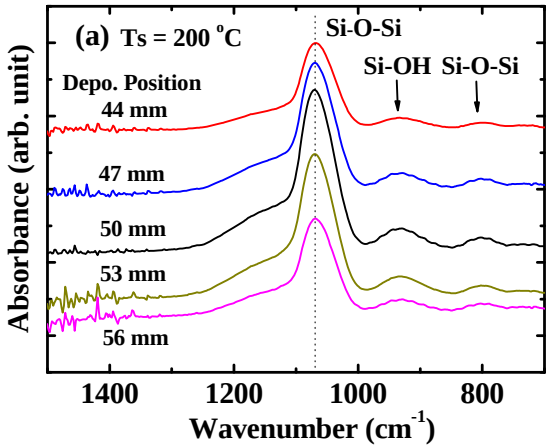
(a) Ts = 200 °C
Si-O-Si
Si-OH
Si-O-Si
Depo. Position
44 mm
47 mm
50 mm
53 mm
56 mm
Absorbance (arb. unit)
1400
1200
1000
800
Wavenumber (cm-1)

Fig. 5(a)

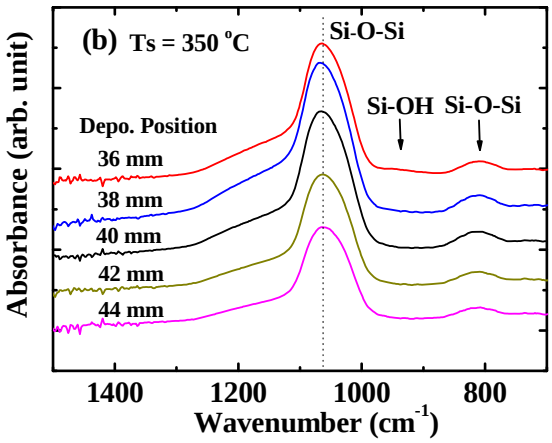
(b) Ts = 350 °C
Si-O-Si
Si-OH
Si-O-Si
Depo. Position
36 mm
38 mm
40 mm
42 mm
44 mm
Absorbance (arb. unit)
1400
1200
1000
800
Wavenumber (cm-1)

Fig. 5(b)

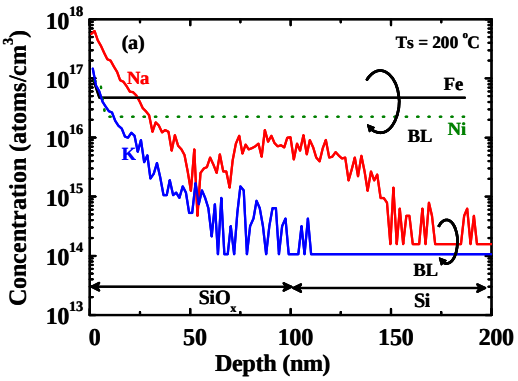
(a)
Ts = 200 °C
Na
K
Fe
Ni
BL
BL
SiOx
Si
Concentration (atoms/cm3)
Depth (nm)
10^18
10^17
10^16
10^15
10^14
10^13
0
50
100
150
200

Fig. 6(a)

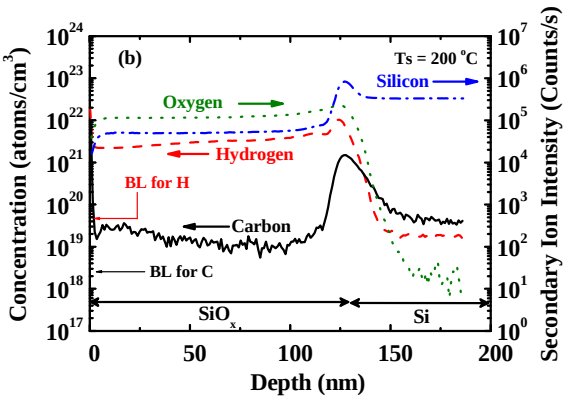
(b)
Ts = 200 °C
Silicon
Oxygen
Hydrogen
BL for H
Carbon
BL for C
SiO$_x$
Si
Concentration (atoms/cm^3)
Secondary Ion Intensity (Counts/s)
Depth (nm)
0
50
100
150
200

Fig. 6(b)

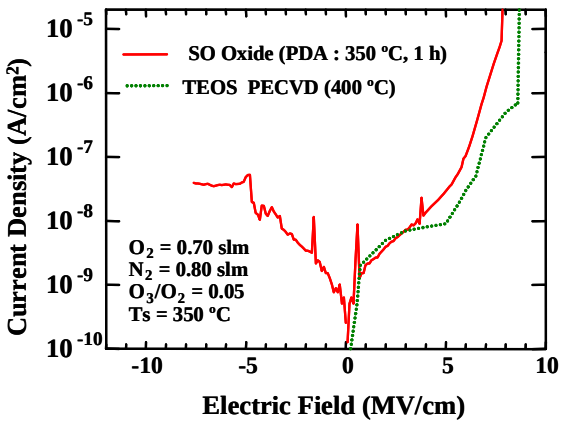
SO Oxide (PDA : 350 °C, 1 h)
TEOS PECVD (400 °C)
O2 = 0.70 slm
N2 = 0.80 slm
O3/O2 = 0.05
Ts = 350 °C
Current Density (A/cm2)
Electric Field (MV/cm)
10-5
10-6
10-7
10-8
10-9
10-10
-10
-5
0
5
10

Fig. 7

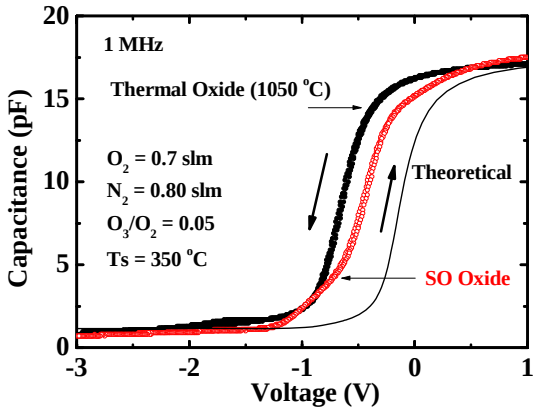
1 MHz
Thermal Oxide (1050 °C)
O2 = 0.7 slm
N2 = 0.80 slm
O3/O2 = 0.05
Ts = 350 °C
Theoretical
SO Oxide
Capacitance (pF)
Voltage (V)
20
15
10
5
0
-3
-2
-1
0
1

Fig. 8

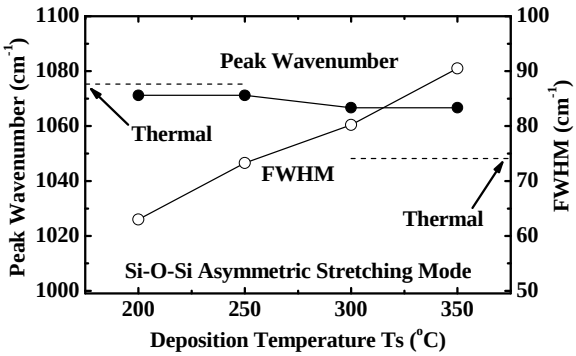
Peak Wavenumber
Thermal
FWHM
Thermal
Si-O-Si Asymmetric Stretching Mode
Peak Wavenumber (cm-1)
FWHM (cm-1)
Deposition Temperature Ts (°C)
1100
1080
1060
1040
1020
1000
100
90
80
70
60
50
200
250
300
350

Fig. 9